Brief Report

DOI: 10.5582/irdr.2021.01004

A novel *BICD2* mutation of a patient with Spinal Muscular Atrophy Lower Extremity Predominant 2

Munkhtuya Tumurkhuu[1,2,*], Uranchimeg Batbuyan[2], Satoru Yuzawa[3], Yanjinlkham Munkhsaikhan[2], Ganbayar Batmunkh[4], Wataru Nishimura[1]

[1] Department of Molecular Biology, International University of Health and Welfare, School of Medicine, Narita, Chiba, Japan;
[2] Department of Genetics and Molecular Biology, School of Bio-Medicine, Mongolian National University of Medical Sciences, Mongolia;
[3] Department of Biochemistry, International University of Health and Welfare, School of Medicine, Narita, Chiba, Japan;
[4] Laboratory of Medical Genetics, National Center of Maternal and Child Health, Mongolia.

SUMMARY The bicaudal D homolog 2 (*BICD2*) gene encodes a protein required for the stable complex of dynein and dynactin, which functions as a motor protein working along the microtubule cytoskeleton. Both inherited and *de novo* variants of *BICD2* are reported with autosomal dominant spinal muscular atrophy with lower extremity predominance (SMALED2). Here, we report a male patient with a novel mutation in the *BICD2* gene caused by a heterozygous substitution of arginine with cysteine at residue 162 (Arg162Cys); inherited from his asymptomatic mother. The patient showed typical clinical symptoms of SMALED2, which was genetically confirmed by sequencing. The Arg162Cys mutant clusters with four previously reported variants (c.361C>G, p.Leu121Val; c.581A>G, p.Gln194Arg; c.320C>T, p.Ser107Leu; c.565A>T, p.Ile189Phe) in a region that binds to the dynein-dynactin complex (DDC). The BICD2 domain structures were predicted and the Arg162Cys mutation was localized in the N-terminus coiled-coil segment 1 (CC1) domain. Protein modeling of BICD2's CC1 domain predicted that the Arg162Cys missense variant disrupted interactions with dynein cytoplasmic 1 heavy chain 1 within the DDC. The mutant did this by either changing the electrostatic surface potential or making a broader hydrophobic unit with the neighboring residues. This hereditary case supports the complex and broad genotype-phenotype correlation of *BICD2* mutations, which could be explained by incomplete penetrance or variable expressivity in the next generation.

Keywords novel mutation, Arg162Cys, dynein-dynactin complex, coiled coil structure

1. Introduction

Spinal muscular atrophy (SMA) is a diverse group of diseases characterized by muscle weakness and atrophy. This is caused by the degeneration of anterior horn cells in the spinal cord, which is also a leading genetic cause of infant death (*1*). The most common form of SMA is caused by the survival of motor neuron 1 (*SMN1*) genes homozygous mutations or deletions in 5q13.1. These are inherited in an autosomal recessive manner and termed SMA5q (*2*).

The SMA5q disease has been classified into four types by order of increasing age and decreasing clinical severity: childhood-onset of SMA type I (MIM #253300), type II (MIM #253550), type III (MIM #253400), and adult-onset of SMA type IV (MIM #271150). Type I SMA is the most severe form with patients having generalized muscle weakness or hypotonia, and a disease onset within the first 6 months of life. Disease severity of SMA5q is found to correlate with oligomerization of SMN and the number of SMN2 gene copies methylated at positions −290 and −296 (*3,4*). In contrast, non-5q SMAs are genetically heterogeneous and phenotypically diverse. They are usually classified by their mode of inheritance (autosomal dominant, recessive, or X-linked) and through their distribution of muscle weakness (proximal, distal, or bulbar) (*5*).

Spinal muscular atrophy with lower limb predominance (SMALED) is an early onset static or slowly progressive disorder. It is best characterized by proximal muscle weakness and atrophy that predominantly affects the lower extremities, with no detectable upper extremity weakness or atrophy (*6,7*). Autosomal dominant SMAs account for < 2% of cases, including SMALED type I and II caused by heterozygous mutations in dynein cytoplasmic 1 heavy chain 1 (*DYNC1H1*) and *BICD2*, respectively (*7,8*). Both genes encode proteins that are part of the dynein-

dynactin complex (DDS). Muscle weakness and atrophy predominantly affect the proximal lower limbs, although involvement of the upper limb and distal lower limb may also occur. In addition, some patients may also demonstrate mild upper motor signs and foot deformities such as high-arched foot, rotated toes, or areflexia of the lower limbs (*9-11*). To date, 30 families with SMALED2 have been reported, carrying 17 missense mutations, including four different mutations in the CC1-dynein binding region (*8-10,12-14*).

Here, we describe a boy who has been clinically diagnosed with a proximal SMA at the age of five, *via* genetic analysis. Molecular analysis revealed a novel missense variant (c.484C>T, Arg162Cys) in exon 3 of *BICD2* in both the boy's and mother's samples.

2. Materials and Methods

2.1. Clinical characteristics of the patient

The proband was a five-year-old boy with movement difficulties, whose family had approached the Department of Genetics and Molecular Biology, in the Mongolian National University of Medical Sciences (MNUMS), to seek medical consultation five years ago. He was born to healthy non-consanguineous parents, and his biological brothers were not clinically affected. The proband's age at symptom onset, walking pattern, and family history were investigated. He has had frequent falls and difficulty in running, jumping, and climbing stairs since he was three years of age. While walking, he showed a waddling gait and Gowers' sign (Figure 1A, 1C).

Intellectual development and physical growth were within normal range. Neurological examination revealed dystrophy of the lower distal limb muscles, reduced deep tendon reflex at the knee, and absent deep tendon reflex at the ankle. The big toe rotated and pointed towards the other toes, and lumbar hyperlordosis was observed (Figure 1A, 1B). Due to the clinical symptoms; electroencephalography, spinal magnetic resonance imaging (MRI) and electromyography were performed. His myelography and spinal MRI results showed normal findings. Motor nerve conduction studies, including speed and amplitude of motor nerve conduction velocity (NCV) and compound muscle action potential, showed results within the normal range. Electromyography showed chronic neurogenic changes in the tibialis anterior and abductor hallucis muscles.

Based on these findings, he was diagnosed clinically with a sporadic SMA and was followed up once a year for the last five years. A recent examination was done in October, 2020 at the age of 10, which revealed a worsening phenotype; the patient was unable to walk without support nor stand-alone for more than ten seconds (Figure 1C). Now, he uses walking aids in two hands.

2.2. Genome isolation and sequencing

After obtaining informed consent, peripheral blood samples were collected from the proband's family, including the parents and two brothers. Both parents of the affected child and unaffected siblings were voluntarily accepted to participate in this study and publish it. All procedures were reviewed and approved by the Ethical Review Committee of MNUMS. All the clinical investigations are in accordance with the Declaration of Helsinki.

Genomic DNA was isolated from 5 mL of the participants' peripheral blood, using a QIAamp DNA mini kit (QIAGEN, Hilden, Germany). Control DNA was obtained from 50 healthy Mongolian individuals. Primer pairs were designed to amplify exons, exon and intron boundaries, and short intron flanking stretches based on primer 3.0 application. The products were sequenced on an ABI Prism 310 automated DNA sequencer (Applied Biosystems, Foster City, CA).

2.3. In-silico analysis of protein structure

The clinical significance of the detected variation was screened using the single nucleotide polymorphism database and the Human Gene Mutation Database. To predict possible effects of the protein mutations, the PolyPhen-2, Sorting Intolerant from Tolerant (SIFT), and Mutation taster software were used in this study. Clinical symptoms of this variant were submitted to ClinVar in March 2020 (accession number VCV000916026.1). The

Figure 1. Clinical features of the proband. (A) The proband at the age of 5 years. Marked atrophy of the lower limb muscles, lumbar lordosis and a waddling gait. **(B)** The proband at age of 10 years. Big toe rotated and pointed towards other toes. **(C)** Step-wise movement of the proband at the age of 10. Waddling gait and Gowers' sign were deepened.

prediction of coiled coil domains in BICD2 proteins was performed using Coiled Coils ExPASy. Protein modeling of BICD2 was performed based on 1c1g (protein data bank -PDB) and interactions with the dynein-dynactin complex were revealed based on the cryo-electron microscopic structure of dyneins bound to dynactin and BICD1R (PDB code 6F1T) or BICD2 (PDB code 6F3A) using the SWISS-MODEL and *PyMOL* web servers (*15,16*). Solvent accessible surface area (SASA) of each residue was calculated using the GetArea program (Sealy Center for Structural Biology, USA) and the location within the heptad structure was modeled by MARCOIL (MPI BioInformatics toolkit).

3. Results and Discussion

We first analyzed all coding regions of the *SMN1* gene in the proband's sample and did not detect any mutations. Next, sequencing was performed by screening for a *BICD2* mutation in exons 2, 3, and 6; where mutations have previously been reported (*5,8-10,17*). A novel heterozygous missense variant, c.484C > T (Arg162Cys) in the *BICD2* gene was found in exon 3. This variant was predicted to be pathogenic by susceptibility prediction sites such as SIFT (0-deleterious), PolyPhen-2 (0.9175-possibly damaging), Mutation Taster (disease-causing mutation with probability- 0.9999), and Grantham Matrix (chemical dissimilarity as radical-180 scores). The Arg162Cys variant was inherited from his mother, with his siblings and father do not have the heterozygous allele. This variant is a novel mutation of *BICD2* and it was not found in 50 Mongolian control subjects.

The Bicaudal D gene is evolutionarily conserved from flies to humans and is localized in chromosomal region 9q22.3, and encodes BICD proteins (*8*). To date, 17 pathogenic missense *BICD2* variants have been described in the medical literature (*10,11,18*) and 95 heterozygous *BICD2* variants with an SMA phenotype have been reported in ClinVar mutants (Figure 2A). These SMA-related cases are equally distributed among domains of *BICD2*, and clinical characteristics of the disease could vary widely, ranging from asymptomatic to lethal congenital manifestations within the same family (*10,18,19*). Our proband showed a typical SMALED2 phenotype; slow progressive weakness affecting only the lower extremities were observed in his early childhood. However, the mother did not show any symptoms.

In mammals, there are two *BICD* homologs (*BICD1* and *BICD2*), whereas there is only one in invertebrates (*10,20*). BICD proteins are comprised of three putative coiled-coil domains, with multiple heptad repeats (*21*). BICD2 coiled-coil domains were predicted using Coiled Coil ExPASy software, showing five potential coiled-coil domains. These were CC1a residues 97-131, CC1b residues 161-310, CC2a residues 381-450, CC2b residues 482-569, and CC3 residues 712-845. Moreover, the coiled-coil probabilities of the domains were 0.99 (CC1a), 0.99 (CC1b), 0.97 (CC2a), 0.82 (CC2b), and 0.87 (CC3) (Figure 2A). The Arg162 residue was localized in the CC1b domain, which in turn was included in the N-terminal domain (residues 25-400) of BICD2. As reported previously, the CC1 domain involves direct binding to both dynein heavy chain-1 and dynactin subunit 2 and promotes the stable interaction between dynein and dynactin. This stability in the DDC complex forms a highly processed microtubule motor (*21,22*). The c.484 C>T (Arg162Cys) in the CC1b domain in BICD2 has previously not been described as a spinal muscular atrophy case, moreover, it is not clear how this mutation results in the interaction of BICD2 within the DDC. To further explore this issue, we constructed a model of the CC1 domain of BICD2 protein using the SWISS model, which we based on the PDB structure 1c1g (Figure 3C, 3D). This protein structure comprised of the CC1 region of the BICD2 protein, consisting of amino acids 15-263. Previously, the physical properties of the coiled-coil domains of heptad breaks were defined by their interactions with the environment and divided into seven positions within three groups: the core unit (a and d), the outfield unit (b, c, and f), and the medium unit (e and g) (*23*). To determine the coiled coil repeats, we assigned the heptad register along the CC1 region, where Arg162 occupied a surface-exposed position on the coiled-coil dimer. On the register this was in position "g" with a probability of 96.5% that it was in the medium unit (Figure 3C, Table 1). Interactions between a and d, and g and e account for the most structural specificity; for instance, switching the position of specific sidechains in the core unit can cause oligomers to switch into trimeric or tetrameric structures (*24*). Similar to the core unit, the residues in the medium unit (e and g) can also alter the oligomeric state of the protein. Specifically, if they include hydrophilic residues in one of the positions, they build dimers rather than trimers or tetramers (*25*). Therefore, when Arg162, a hydrophilic positively charged residue, is mutated into Cys162, the BICD2 configuration might be converted from dimeric to a different geometric structure. Additionally, a side chain of Arg162 was closely detected with neighboring chains Gln159 and Asp166 in position "d" in the protein model. This interaction could be disrupted when it is mutated into Cys162, resulting in the abolition of these bonds. Furthermore, it could cause changes in the electrostatic surface potential, making a broader hydrophobic unit with two seams of core residues; "g" and "d", "Cys162" and "Gln159", respectively (Figure 3C, 3D). These predicted coiled-coil structure disruptions could lead to dysfunctional interactions between the N-terminal segment of the BICD2 protein and dynein-dynactin. In line with our prediction, a comprehensive set of polar mutations are located in

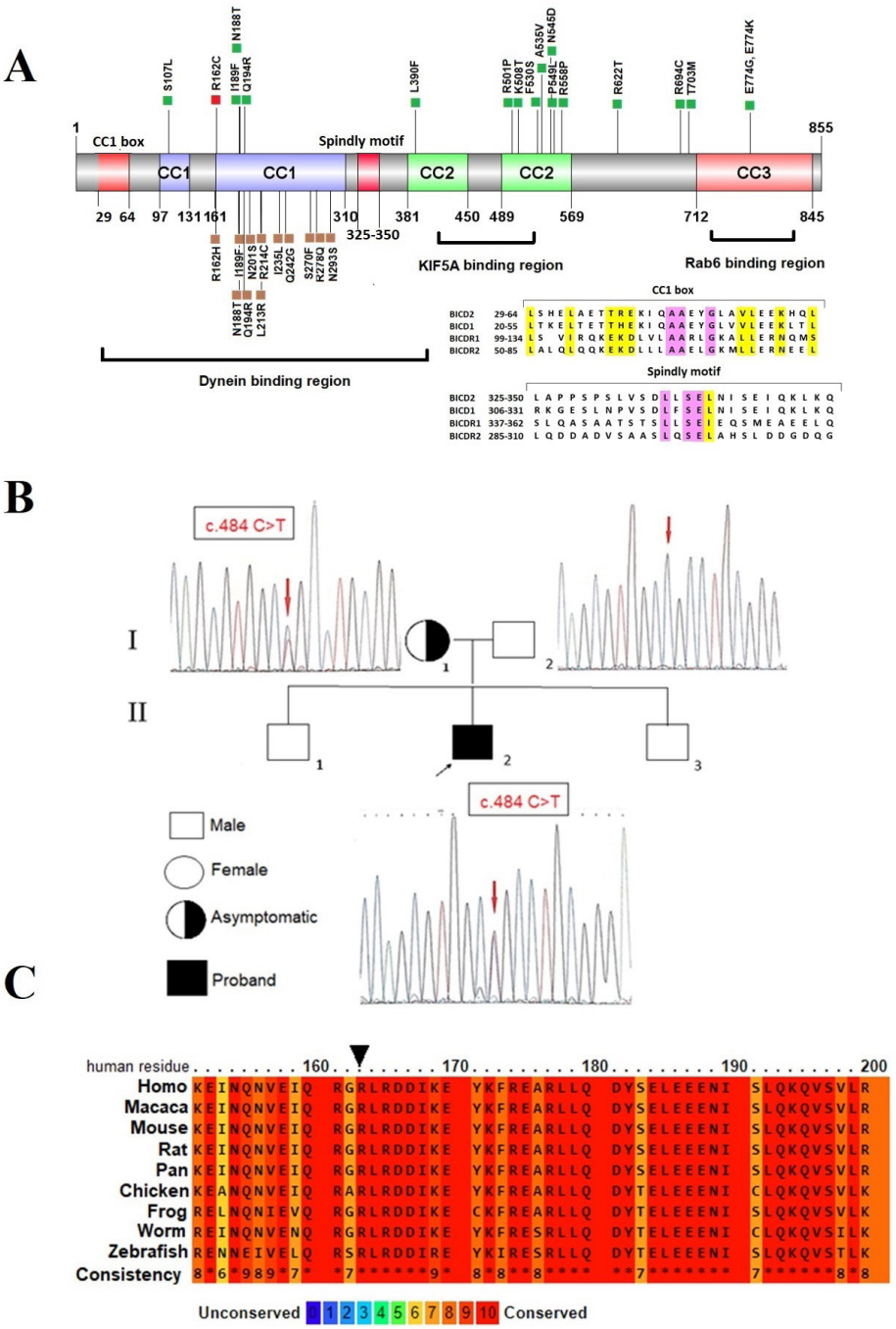

Figure 2. Location, conservation and sequencing of the R162C variant. (A) Green dots represent pathogenic cases, brown dots represent clinical cases, which are reported in the ClinVar database as of June, 2020. The R162C variant is shown in red. BCID2 protein structure, coiled coil domains were identified as CC1a, residues 97-131, CC1b residues 161-310, CC2a residues 381-450, CC2b residues 482-569 and CC3 residues 712-845 (Coiled coil -ExPASy). Sequence alignment of CC1 box (Ala-Ala-x-x-Gly; x-any amino acid) and Spindly motif (Leu-x-Ser-Glu-x; x-any amino acid) of BICD family are shown (*27*). The binding regions of dynein, KIF5A and Rab6 were defined as reported previously (*22,29*). **(B)** Identification of a heterozygous mutation in *BICD2* gene of the parents and son by Sanger sequencing. **(C)** Interspecies alignment of the BICD2 protein harboring the Arg162 residue. The lower panel indicates the conservation score in color code. Black arrow represents the location of Arg162. Aligned species were *Homo sapiens, Macaca mulatta* (rhesus macaque), *Mus musculus* (mouse), *Rattus norvegicus* (rat), *Pan troglodytes* (chimpanzee), *Gallus gallus* (chicken), *Xenopus tropical* (frog), *Thamnophis elegans* (worm) and *Danio rerio* (zebrafish).

positions "e" and "g". This brings a structural diversity to BICD2 and these residues flank the hydrophobic core, resulting in the formation of heterodimers between these positions and the disruption of DDC binding (*26*).

Furthermore, we used protein models (PDB codes 6F1T and 6F3A) to determine the interaction between the Arg162 residue, found on the N-terminus of BICD2, and DDC (*15,16*). Recent studies have shown that other adapters such as BICD family like cargo adapter 1 (BICDR1), Rab6, and HOOK3 are generally unrelated at the sequence level, but they all share regions termed the CC1 box (consensus sequence: Ala-Ala-x-x-Gly;

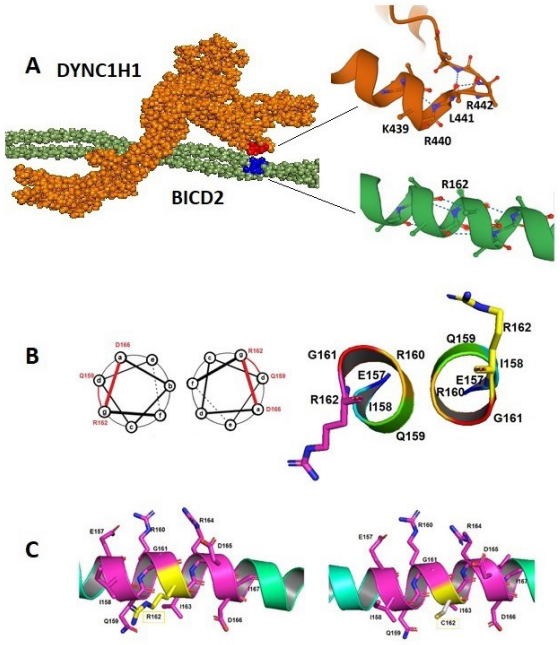

Figure 3. Structural analysis of the position of Arg162 in BICD2. (A) The N terminal part of BICD2 protein is shown as a rope-like structure, highlighted in pink and residues 158-164 of BICD2 spotted as blue dots. DYNC1H1 is represented by a green color and interaction site with BICD2 is colored red. This red site contains residues 436-441 of DYNC1H1 (PDB 6F3A). **(B)** Helical-wheel diagram showing how the heptad repeat *abcdefg* track around helical structure and among them, Arg162 is in the position of "g". **(C)** Representation of the structure of neighboring five residues of Arg162, modelled on the crystal structure from tropomyosin (PDB 1C1G) shown in pink. The Arg162 and Cys162 are shown in yellow.

x-any amino acid) and Spindly motif (Leu-x-Ser-Glu-x; x-any amino acid) to interact with both dynein and dynactin (*27*) (Figure 2A). To date, a high-resolution model of BICD2 has not been reported, and the 6F1T (chain X) structure is the only available high-resolution model of BICDR1's N-terminal region interacting with the DDC. We localized the position of Arg162 of BICD2 to Arg250 of BICDR1 by aligning sequences of the CC1 box and Spindly motif of BICD family proteins (Figure 2A). Arg250 of BICDR1 (PDB code 6F1T) aligned with an amino acid at position 139 of BICD2 (PDB code 6F3A), whereas it would be at residue Arg162 in our research. Arg162 of BICD2 interacted closely with the residues of DYNC1H1 at positions Val438, Lys439, Ar440, and Lys441 (Figure 3A). Residues 441-454 were predicted to be loose strands in the heavy chain domain of DYNC1H1. We found that residues 435-443 of the DYNC1H1 protein interacted with residues 249-256 of BICDR1, enabling the connection of these proteins (Figure 3B). We predicted that these interactions might be necessary for the recruitment of dynein into cargo molecules of BICDR1 or BICD2 to form the DDC. Consistent with our research, high-resolution analysis of DYNC1H1 showed that it has two binding sites with BICDR1. The first site interacts extensively with BICDR1, however the second site is not directly connected, but instead touches the density that packs the coiled coil regions of BICDR1 (*28*). The location of Arg162, which corresponds to Arg250 of BICDR1, was in the second binding site of the DDC, suggesting that

Table 1. Mutations located in CC1 domain of BICD2 associated with spinal muscular atrophy

Residues	SASA%	B/E	Heptad position, (%)	Conserved score	Phenotype	ClinVar №
E101K	68.2	E	*e* (51.8)	10	SMALED2	VCV000541286
S107L	16.8	B	*c* (51.8)	10	SMALED2	VCV000055857
					Distal hereditary motor neuropathy	
L119I	75.7	E	*b* (99.8)	10	SMALED2	VCV000424580
T123M	67.5	E	*f* (99.8)	10	SMALED2	VCV000664075
E124D	44.7	-	*g* (99.8)	9	SMALED2	VCV000654487
N130S	79.7	E	*f* (99.8)	10	SMALED2	VCV000641810
R162H	84.0	E	*g* (96.5)	10	SMALED2	VCV000565772
N188T	22.5	-	*a* (93.1)	10	SMALED2	VCV000055859
I189F	59.1	E	*b* (93.1)	10	Distal hereditary motor neuropathy	VCV000637065
Q194R	68.4	E	*g* (93.1)	10	SMALED2	VCV000617527
S196F	82.5	E	*b* (88.3)	10	SMALED2	VCV000851654
N201S	44.6	-	*d* (92.7)	7	SMALED2	VCV000423894
K213R	62.0	E	*b* (100.0)	8	SMALED2	VCV000453157
R214C	67.7	E	*c* (100.0)	10	SMALED2	VCV000474279
I235L	57.3	E	*c* (100.0)	10	SMALED2	VCV000638377
R238Q	60.4	E	*f* (100.0)	10	SMALED2	VCV000573134
E242G	59.5	E	*c* (100.0)	10	SMALED2	VCV000474280
K254R	26	-	*b* (100.0)	10	Hereditary spastic paraplegia	VCV000424684

SASA% (Solvent accessible surface area %): percentage of each residue that is accessed by solvent was calculated with GetArea program. **B/E**: Buried or exposed to the solvent. Residues are considered if SASA% is less than 20% and to be solvent exposed if SASA% is more than 50%. **Heptad position, (%)**: The heptad sructure was calculated by MARCOIL (MPI BioInformatics toolkit) and the probabilty from 0 to 100%. **Conserved score**: The conserved scoring was performed by PRALINE. The scoring scheme works from 0 for the least conserved alignment position, up to 10 for the most conserved alignment position. Aligned species were *Homo sapiens, Macaca mulatta* (rhesus macaque), *Mus musculus* (mouse), *Rattus norvegicus* (rat), *Pan troglodytes* (chimpanzee), *Gallus gallus* (chicken), *Xenopus tropical* (frog), *Thamnophis elegans* (worm) and *Danio rerio* (zebrafish). **Phenotype**: Spinal muscular atrophy-like phenotypes were reported in ClinVar 2020 by June, 2020.

it would increase the flexibility of DDC.

Previous work in BICDR1 showed that recruitment of two dynein molecules alongside shorter molecules of BICD homology proteins, resulted in faster motility of the DDC, thus increasing its velocity (*28*). Unlike BICD2, BICDR1 recruits two dyneins, moreover, a mutational switch in the position of the N-terminal region of BICD2 is sufficient to recruit a second dynein (*15,16*). BICD2's larger size, and a recruitment site mutation in the DDC could both disrupt the recruitment of the complex or change the electrophysiological bond around important residues, which in turn might cause a more indirect or slower route along the microtubule when compared with BICDR1. Furthermore, the minimal side chain of Cys162 could account for reduced binding to the DDC, because cysteine has a smaller side chain than arginine. In addition, the mother of the proband did not show any of the clinical symptoms of SMALED2. This supports the complex and broader genotype-phenotype correlation of *BICD2* mutations that include both incomplete penetrance and variable expressivity in the next generation.

In conclusion, autosomal dominant SMALED type II is a rare entity with few cases reported in the literature, but it is important for clinicians to be familiar with this disease because of its broad phenotypic expression. Mechanisms leading to variable expressivity and onset of SMALED2 could be explained by alterations in molecular interactions between the domains of BICD2 and the DDC. Thus, suggesting the presence of genetic mutations that act as molecular units of protein structure can alter phenotypic expressivity of the disease.

Acknowledgements

We thank the family members for taking part in this study. We thank all members of Department of Genetics and Molecular biology, School of Bio-Medicine, MNUMS for critical comments and supports. This research work is a part of M.Sc. work of Uranchimeg Batbuyan, MNUMS Mongolia.

Funding: This research was funded by International University of Health and Welfare, Chiba, Japan from 2020-2021.

Conflict of Interest: The authors have no conflicts of interest to disclose.

References

1. Lefebvre S, Bürglen L, Reboullet S, *et al.* Identification and characterization of a spinal muscular atrophy-determining gene. Cell. 1995; 80:155-165.
2. Li W. How do SMA-linked mutations of SMN1 lead to structural/functional deficiency of the SMA protein? PLoS One. 2017; 12:1-13.
3. Hauke J, Riessland M, Lunke S, Eyüpoglu IY, Blümcke I, El-osta A, Wirth B, Hahnen E. Survival motor neuron gene 2 silencing by DNA methylation correlates with spinal muscular atrophy disease severity and can be bypassed by histone deacetylase inhibition. Hum Mol Genet. 2009; 18:304-317.
4. Lorson CL, Hahnen E, Androphy EJ, Wirth B. A single nucleotide in the SMN gene regulates splicing and is responsible for spinal muscular atrophy. Proc Natl Acad Sci U S A. 1999; 96:6307-6311.
5. Peeters K, Chamova T, Jordanova A. Clinical and genetic diversity of SMN1-negative proximal spinal muscular atrophies. Brain. 2014; 137:2879-2896.
6. Harms MB, Allred P, Gardner R, Fernandes Filho JA, Florence J, Pestronk A, AI-Lozi M, Baloh RH. Dominant spinal muscular atrophy with lower extremity predominance: Linkage to 14q32. Neurology. 2010; 75:539-546.
7. Harms MB, Ori-McKenney KM, Scoto M, *et al.* Mutations in the tail domain of DYNC1H1 cause dominant spinal muscular atrophy. Neurology. 2012; 78:1714–1720.
8. Neveling K, Martinez-Carrera LA, Hölker I, *et al.* Mutations in BICD2, which encodes a golgin and important motor adaptor, cause congenital autosomal-dominant spinal muscular atrophy. Am J Hum Genet. 2013; 92:946-954.
9. Synofzik M, Martinez-Carrera LA, Lindig T, Schöls L, Wirth B. Dominant spinal muscular atrophy due to BICD2: A novel mutation refines the phenotype. J Neurol Neurosurg Psychiatry. 2014; 85:590-592.
10. Oates EC, Rossor AM, Hafezparast M, *et al.* Mutations in BICD2 cause dominant congenital spinal muscular atrophy and hereditary spastic paraplegia. Am J Hum Genet. 2013; 92:965-973.
11. Rossor AM, Oates EC, Salter HK, *et al.* Phenotypic and molecular insights into spinal muscular atrophy due to mutations in BICD2. Brain. 2015; 138:293-310.
12. Storbeck M, Eriksen BH, Unger A, Hölker I, Aukrust I, Martínez-Carrera LA, Linke WA, Ferbert A, Heller R, Vorgerd M, Houge G, Wirth B. Phenotypic extremes of BICD2-opathies: From lethal, congenital muscular atrophy with arthrogryposis to asymptomatic with subclinical features. Eur J Hum Genet. 2017; 25:1040-1048.
13. Yoshioka M, Morisada N, Toyoshima D, Yoshimura H, Nishio H, Iijima K, Takeshima Y, Uehara T, Kosaki K. Novel *BICD2* mutation in a Japanese family with autosomal dominant lower extremity-predominant spinal muscular atrophy-2. Brain Dev. 2018; 40:343-347.
14. Rossor AM, Oates EC, Salter HK, *et al.* Reply: The p.Ser107Leu in BICD2 is a mutation "hot spot" causing distal spinal muscular atrophy. Brain. 2015; 138:e392.
15. Urnavicius L, Lau CK, Elshenawy MM, Morales-Rios E, Motz C, Yildiz A, Carter AP. Cryo-EM shows how dynactin recruits two dyneins for faster movement. Nature. 2018; 554:202-206.
16. Urnavicius L, Zhang K, Diamant AG, Motz C, Schlager MA, Yu M, Patel NA, Robinson CV, Carter AP. The structure of the dynactin complex and its interaction with dynein. Science. 2015; 347:1441-1446.
17. Rossor AM, Sleigh JN, Groves M, Muntoni F, Reilly MM, Hoogenraad CC, Schiavo G. Loss of BICD2 in muscle drives motor neuron loss in a developmental form of spinal muscular atrophy. BioRxiv. 2019; 6:854711.
18. Oates EC, Reddel S, Rodriguez ML, Gandolfo LC, Bahlo

M, Hawke SH, Lamandé SR, Clarke NF, North KN. Autosomal dominant congenital spinal muscular atrophy: A true form of spinal muscular atrophy caused by early loss of anterior horn cells. Brain. 2012; 135:1714-1723.
19. Ravenscroft G, Di Donato N, Hahn G, Davis MR, Craven PD, Poke G, Neas KR, Neuhann TM, Dobyns WB, Laing NG. Recurrent *de novo* BICD2 mutation associated with arthrogryposis multiplex congenita and bilateral perisylvian polymicrogyria. Neuromuscul Disord. 2016; 26:744-748.
20. Terenzio M, Schiavo G. The more, the better: The BICD family gets bigger. EMBO J. 2010; 29:1625-1626.
21. Hoogenraad CC, Akhmanova A, Howell SA, Dortland BR, De Zeeuw CI, Willemsen R, Visser P, Grosveld F, Galjart N. Mammalian golgi-associated Bicaudal-D2 functions in the dynein-dynactin pathway by interacting with these complexes. EMBO J. 2001; 20:4041-4054.
22. Splinter D, Razafsky DS, Schlager MA, Serra-Marques A, Grigoriev I, Demmers J, Keijzer N, Jiang K, Poser I, Hyman AA, Hoogenraad CC, King SJ, Akhmanova A. BICD2, dynactin, and LIS1 cooperate in regulating dynein recruitment to cellular structures. Mol Biol Cell. 2012; 23:4226-4241.
23. Tanizawa H, Ghimire GD, Mitaku S. A high performance prediction system of coiled coil domains containing heptad breaks: SOSUIcoil. Chem-Bio Informatics J. 2008; 8:96-111.
24. Harbury PB, Kim PS AT. Crystal structure of an isoleucine-zipper trimer. Nature. 1994; 1:80-83.
25. Woolfson DN, Bartlett GJ, Bruning M, Thomson AR. New currency for old rope: From coiled-coil assemblies to α-helical barrels. Curr Opin Struct Biol. 2012; 22:432-441.
26. Keating AE, Malashkevich VN, Tidor B, Kim PS. Side-chain repacking calculations for predicting structures and stabilities of heterodimeric coiled coils. Proc Natl Acad Sci U S A. 2001; 98:14825-14830.
27. Gama JB, Pereira C, Simões PA, Celestino R, Reis RM, Barbosa DJ, Pires HR, Carvalho C, Amorim J, Carvalho AX, Cheerambathur DK, Gassmann R. Molecular mechanism of dynein recruitment to kinetochores by the Rod-Zw10-Zwilch complex and Spindly. J Cell Biol. 2017; 216:943-960.
28. Schroeder CM, Vale RD. Assembly and activation of dynein-dynactin by the cargo adaptor protein Hook3. J Cell Biol. 2016; 214:309-318.
29. Liu Y, Salter HK, Holding AN, Johnson CM, Stephens E, Lukavsky PJ, Walshaw J, Bullock SL. Bicaudal-D uses a parallel, homodimeric coiled coil with heterotypic registry to coordinate recruitment of cargos to dynein. Genes Dev. 2013; 27:1233-1246.

Received January 8, 2021; Revised March 16, 2021; Accepted March 25, 2021.

**Address correspondence to:*
Munkhtuya Tumurkhuu, Department of Molecular Biology, School of Medicine, International University of Health and Welfare, 4-3 Kozunomori, Narita, Chiba 286-8686, Japan.
E-mail: munkhtuya.t@iuhw.ac.jp, munkhtuya.tumurkhuu@gmail.com

Released online in J-STAGE as advance publication March 31, 2021.